ACS SyntheticBiology

pubs.acs.org/synthbio

Research Article

# *In Situ* Biomanufacturing of Small Molecules in the Mammalian Gut by Probiotic *Saccharomyces boulardii*

Deniz Durmusoglu,[⊥] Ibrahim S. Al'Abri,[⊥] Scott P. Collins, Junrui Cheng, Abdulkerim Eroglu, Chase L. Beisel, and Nathan Crook*

Cite This: *ACS Synth. Biol.* 2021, 10, 1039–1052

Read Online

ACCESS | Metrics & More | Article Recommendations | Supporting Information

**ABSTRACT:** *Saccharomyces boulardii* is a probiotic yeast that exhibits rapid growth at 37 °C, is easy to transform, and can produce therapeutic proteins in the gut. To establish its ability to produce small molecules encoded by multigene pathways, we measured the amount and variance in protein expression enabled by promoters, terminators, selective markers, and copy number control elements. We next demonstrated efficient (>95%) CRISPR-mediated genome editing in this strain, allowing us to probe engineered gene expression across different genomic sites. We leveraged these strategies to assemble pathways enabling a wide range of vitamin precursor (β-carotene) and drug (violacein) titers. We found that *S. boulardii* colonizes germ-free mice stably for over 30 days and competes for niche space with commensal microbes, exhibiting short (1−2 day) gut residence times in conventional and antibiotic-treated mice. Using these tools, we enabled β-carotene synthesis (194 μg total) in the germ-free mouse gut over 14 days, estimating that the total mass of additional β-carotene recovered in feces was 56-fold higher than the β-carotene present in the initial probiotic dose. This work quantifies heterologous small molecule production titers by *S. boulardii* living in the mammalian gut and provides a set of tools for modulating these titers.

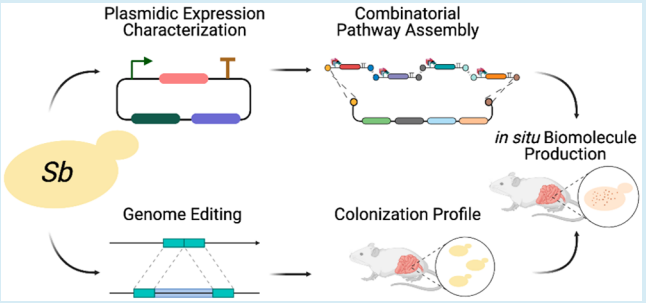


**KEYWORDS:** *Saccharomyces boulardii, probiotic engineering, metabolic engineering, colonization profile, in situ production, β-carotene*



Next-generation engineered probiotics offer unique attributes for treatment of disease.[1] By leveraging decades of advances in metabolic engineering and microbial ecology,[2] these organisms convert unused dietary material to therapeutic molecules directly in the gut.[3−5] Furthermore, integrated sensors enable drug synthesis to be tailored to the severity and location of disease.[6−9] Coupled with the manufacturing and distribution infrastructure in place for traditional probiotics, engineered probiotics promise to reduce drug cost while improving delivery specificity.[10] To date, almost all engineered probiotics have been members of the bacterial domain of life due to their high numerical abundance in the gut[11,12] and ease of engineering.[7,13,14] For example, *Escherichia coli* Nissle 1917 has been engineered to treat phenylketonuria (PKU),[13,15] hyperammonemia,[16] cancer,[17] and bacterial infections.[18] Unfortunately, bacteria are susceptible to antibiotics and bacteriophage,[19] and have difficulty producing high levels of post-translationally modified proteins.[20]

In addition to bacteria, a diverse fungal population exists in the human gut.[21−24] While the number of fungal cells in the gut is much lower than bacteria, fungal cells are ∼100-fold larger, indicating that their biomass and role in the gut may be larger than metagenomic surveys indicate.[23,25] Indeed, commensal fungi play important roles in the development of inflammatory bowel diseases and also provide protective heterologous immunity to pathogens by training the immune system.[26,27] Furthermore, fungi are not susceptible to bacteriophage and are easily engineered to secrete high titers of post-translationally modified proteins. Thus, in this study, we focused on engineering the only fungal probiotic that is approved by the FDA: *Saccharomyces boulardii*.[28]

*S. boulardii* (*Sb*) was originally isolated from lychee and mangosteen in 1923 by Henri Boulard and has been used to treat ulcerative colitis, diarrhea, and recurrent *Clostridium difficile* infection.[29,30] *Sb* is closely related to *Saccharomyces cerevisiae*, indicating that it may be similarly amenable to engineering.[31,32] Supporting this, *S. cerevisiae* (*Sc*) expression vectors can be transformed and propagated in *Sb*, and CRISPR/Cas9-mediated genome editing is functional in both strains.[33] However, compared to *Sc*, *Sb* better tolerates low pH and grows more rapidly at human body temperature.[31,34,35] These properties position *Sb* as a unique chassis for the

**Received:** November 5, 2020
**Published:** April 12, 2021




https://doi.org/10.1021/acssynbio.0c00562
*ACS Synth. Biol.* 2021, 10, 1039−1052

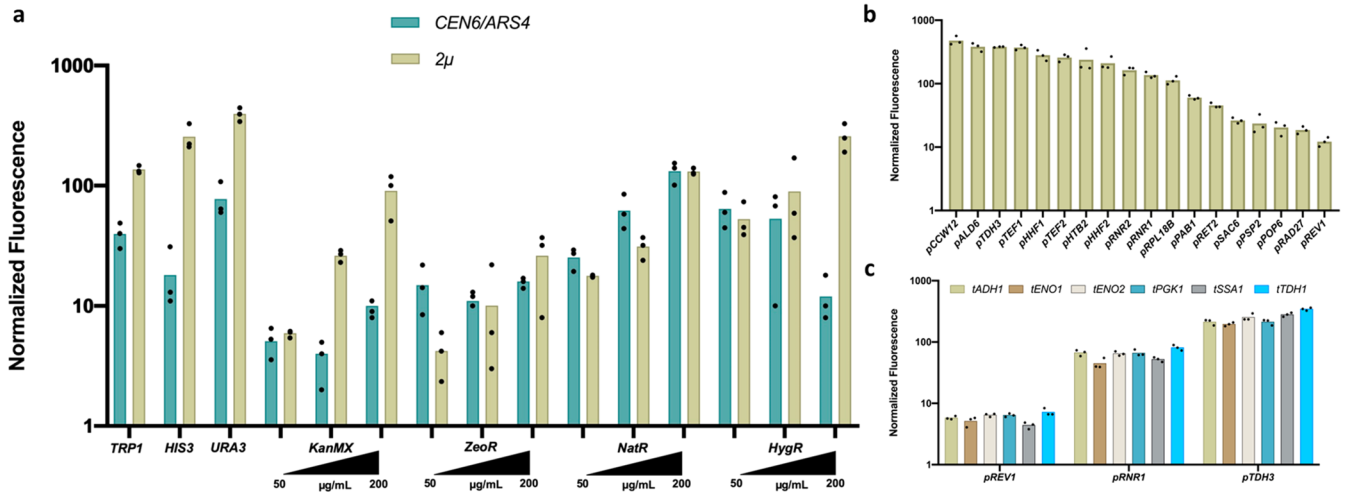


**Figure 1.** Plasmid-based gene expression enabled by *S. boulardii* (a) markers and origins of replication, (b) promoters, and (c) terminators *in vitro*. (a) 3 auxotrophic (*URA3*, *HIS3*, *TRP1*) and 4 antifungal (*KanMX*, *ZeoR*, *NatR*, *HygR*) markers were cloned in plasmids containing the *TDH3* promoter, mRuby2 fluorescent protein and *TDH1* terminator. Centromeric (*CEN6/ARS4*) and episomal (*2μ*) origins were cloned in combination with the 7 selective markers. Plasmids with antifungal markers were tested at 3 different antifungal concentrations (50, 100, and 200 μg/mL). (b) 18 constitutive promoters were cloned 5′ of the *mRuby2* fluorescent protein and the *TDH1* terminator. (c) 5 terminators were cloned 3′ of 3 different promoters at different strengths (*pTDH3*-strong, *pRNR1*-medium and *pREV1*-weak) and the *mRuby2* fluorescent protein. Absolute fluorescence values were obtained *via* flow cytometry for 3 biological replicates ($n$ = 3). Absolute fluorescence values were normalized to fluorescence values of cells harboring the spacer plasmid. The height of the bars represents the normalized mean fluorescence value of 3 biological replicates and the black dots show the normalized mean of each biological replicate.

delivery of therapeutics to the gut. Indeed, *Sb* has been engineered to secrete human synthetic lysozyme[33] and HIV-1 Gag[36] in culture, as well as IL-10, atrial natriuretic peptide, and nanobodies targeting the *C. difficile* toxins in mouse models of disease.[37−39] However, the *in situ* biomanufacturing of small molecules, an important therapeutic group for which yeast possesses distinct advantages relative to bacteria,[40] has not yet been demonstrated for *Sb*. To enable balanced, high metabolic fluxes through small molecule biosynthesis pathways, finely tuned gene expression is critical. Therefore, in this work we sought to elucidate the genetic strategies governing tunable biomolecule production in *Sb*, compare the activities of genetic parts between *Sb* and *Sc*, and compare *in vitro* and *in vivo* small molecule production titers.

We began by performing the most comprehensive analysis of engineered gene expression to date in *Sb*, characterizing a library of *Sc* genetic parts (promoters, selective markers, origins of replication, and terminators)[41] in plasmid-based and genomic contexts. We then applied these parts to construct for the first time *Sb* strains exhibiting high levels of vitamin precursor (*β*-carotene) and drug (violacein) production. Next, we directly compared the residence times of *Sb* in germ-free, antibiotic treated, and conventional mice. Finally, we investigated the colonization profile and biomolecule production capacities of *β*-carotene-producing *Sb* in the mono-colonized mouse gut, demonstrating *in situ* production of a heterologous small molecule for the first time in this strain. This work therefore establishes our ability to engineer *Sb* to produce small molecules in the mammalian gut.

## RESULTS AND DISCUSSION

**Selective Marker and Origin of Replication Tune Gene Expression over a Wide Range.** Due to the genetic relatedness of *Sb* and *Sc*, we first asked whether synthetic parts that are commonly used in *Sc* would function in *Sb*. If so, it would indicate that the large toolbox that has been developed for *Sc* engineering could be applied to probiotic *Sb*. We initially focused on plasmids because they enable rapid prototyping. Unlike the genome, gene expression on plasmids is impacted by the origin of replication and selectable marker.[42] We therefore sought to understand the interplay between origin and marker in determining engineered gene expression in *Sb*. We used a model fluorescent protein (*mRuby2*) to facilitate gene expression measurements, as it exhibited a high signal-to-noise ratio (Figure S1). We generated expression cassettes containing *pTDH3*, *mRuby2*, and *tTDH1* in combination with 7 selective markers (*URA3*, *HIS3*, *TRP1*, *KanMX*, *ZeoR*, *NatR*, and *HygR*) and two origins of replication (*CEN* and *2μ*). The *CEN* we used was derived from *Sc* and differs from the most closely related *Sb CEN* at 5 positions. We transformed the cassettes containing auxotrophic markers into the corresponding auxotrophic strains (*SbΔURA3*, *SbΔHIS3*, and *SbΔTRP1*), and antifungal markers into wild-type *Sb*. We achieved maximum fluorescence using *URA3-2μ* and minimum using *KanMX-CEN* at 100 μg/mL G418, collectively enabling a 100-fold range in gene expression by varying the plasmid "backbone" alone (Figure 1a, Figure S2a). The ability to tune plasmid-based gene expression without changing the promoter may provide a convenient way to modulate biomolecule output while conserving regulatory logic.

**The Impact of the Origin on Gene Expression Is Marker-Dependent.** We next asked whether certain markers or origins had consistent effects on gene expression. For auxotrophic markers, *2μ* always yielded higher fluorescence than *CEN* (two-way ANOVA, $p < 0.05$) (Figure 1a). This is consistent with *Sc*, in which *2μ* plasmids with auxotrophic markers are maintained at 28−58 copies per cell, whereas *CEN* plasmids are maintained at only 4−8 copies per cell.[42] However, apart from *HygR* (two-way ANOVA, $p < 0.0001$), plasmids containing antifungal markers were not impacted by the origin at the antifungal concentrations tested (two-way ANOVA, $p > 0.05$). For the CEN origin, using *NatR* at the


https://doi.org/10.1021/acssynbio.0c00562
ACS Synth. Biol. 2021, 10, 1039−1052

maximum antifungal concentration yielded the highest fluorescence (two-way ANOVA, $p < 0.05$). However, for the $2\mu$ origin, all auxotrophic markers gave higher fluorescence levels than any antifungal marker at the antifungal concentrations tested (two-way ANOVA, $p < 0.0001$). Taken together, our data indicate that gene expression in plasmids containing auxotrophic markers (but not antifungal markers) is sensitive to the choice of origin, and that selective marker significantly impacts gene expression for both *CEN* and $2\mu$ origins. These data collectively point to environmental conditions (*e.g.*, antifungal concentration) as strong mediators of plasmid-based gene expression in *Sb*, indicating that measuring plasmid-based gene expression *in vivo* (where conditions are very different than in shake flasks) in future work would be very interesting.

**Plasmid-based Gene Expression Noise Is Marker- and Origin-Dependent.** Cell-to-cell variability in gene expression can have dramatic impacts on overall production titers.[43] Therefore, it is desirable to design engineered probiotics to exhibit minimal gene expression noise. Previous work in *Sc* showed that cell variability is a function of promoter, terminator, origin, and selective marker.[44] We thus calculated the population-level coefficient of variance (CV) in the fluorescence values we obtained for *Sb*. We found that marker, origin, and marker-origin interactions had significant impacts on expression noise (two-way ANOVA, $p < 0.05$). Specifically, *CEN* plasmids exhibited less cell−cell variability than $2\mu$ plasmids (two-way ANOVA, $p < 0.05$) (Figure S2c). Additionally, expression noise in auxotrophic markers (*TRP1*, *HIS3*, and *URA3*) was similar to each other (two-way ANOVA, $p > 0.05$), while it varied among antifungal markers (Figure S2c). Compared to other selective markers, plasmids with the antifungal marker *ZeoR* had the highest gene expression noise (two-way ANOVA, $p < 0.01$). Increasing the concentration of applied antifungal decreased the gene expression noise (two-way ANOVA, $p < 0.01$) (Figure S2c). These data suggest differences in the ways that the auxotrophic and antifungal markers interact with origins of replication to control gene expression, and offer suggestions for designing genetic circuits that reduce plasmid-based gene expression variance. While our results show that individual *Sb* cells exhibit stochastic gene expression, population coefficients of variance are similar to *Sc* harboring similar plasmids.[45−47] Nevertheless, we believe that the tools developed to reduce gene expression noise in *Sc* such as RNAi, Noise Tuner,[44] and Transcriptional Regulators[48] can be applied to *Sb*. Looking forward, because these measurements were obtained in shake flasks, where conditions are relatively homogeneous, we anticipate that performing future experiments in the gut, with its substantially more numerous environmental niches, would yield higher noise values.

***S. cerevisiae* Promoters Largely Maintain Their Relative Activities in *S. boulardii*.** Next, we quantified the ability of 18 constitutive *Sc* promoters to express *mRuby2* in *Sb*. Each promoter had a homologue in *Sb*, with percent nucleotide identities ranging from 97% to 100% (Table S1). In these experiments, vectors contained the $2\mu$ origin and the *URA3* auxotrophic marker to maximize the range over which changes to fluorescence could be detected (Figure 1a). Each promoter drove the expression of *mRuby2* and transcription was terminated by *tTDH1*. Each promoter yielded different mean fluorescence values (two-way ANOVA, $p < 0.0001$), and these promoters collectively modulated fluorescence levels over a 40-fold range (Figure 1b, Figure S3). While the relative activities of 16/18 promoters in *Sb* were similar to reported values in *Sc* ($R^2 = 0.79$), two promoters (*pALD6* and *pRNR2*) showed 10-fold higher activity in *Sb* than in *Sc* (Figure S4). While the precise roles of these genes in the probiotic properties of *Sb* are unknown, Ald6p is involved in the detoxification of aldehyde molecules to their corresponding acid,[49] and Rnr2p catalyzes the rate-limiting step in dNTP synthesis.[50] Collectively, these data curate a set of promoters enabling precise tuning of gene expression in *Sb*, and indicates that constructs developed for *Sc* will exhibit similar performance in *Sb*.

**Terminators Modulate Gene Expression in a Promoter-Dependent Manner.** Terminators regulate expression in yeast by modulating mRNA stability, translational efficiency and mRNA localization.[51] Furthermore, a terminator's effect on expression can depend on the strength of the promoter or the sequence of the expressed gene.[52,53] Therefore, we were interested in defining the effect of terminator on gene expression in *Sb*. We cloned 6 terminators (*tENO1*, *tENO2*, *tSSA1*, *tPGK1*, *tADH1*, and *tTDH1*) into mRuby2 expression constructs driven by strong (*pTDH3*), medium (*pRNR1*), or weak (*pREV1*) promoters. We found that these terminators could collectively modulate gene expression by 1.77, 1.81, and 1.64-fold in constructs containing *pTDH3* (*tSSA1 vs tTDH1*), *pRNR1* (*tSSA1 vs tTDH1*), or *pREV1* (*tSSA1 vs tTDH1*), effectively increasing the expression range beyond that enabled by varying the promoter alone (40-fold, Figure 1b). In particular, using a strong promoter (*pTDH3*) with *tTDH1* yielded 80-fold higher expression than a weak promoter (*pREV1*) with *tSSA1*. While the total range of expression observed at the population level varied over 3−4 orders of magnitude (Figure S5), the ability to modulate population expression means over an 80-fold range is meaningful, as the total dose of a delivered biomolecule will be directly proportional to this mean. Relative to *tSSA1 and tTDH1*, we found that *tENO1*, *tENO2*, *tADH1*, and *tPGK1* significantly decreased gene expression in constructs containing the strong *pTDH3* promoter (two-way ANOVA, $p < 0.005$) while for *pRNR1* and *pREV1*, the differences in gene expression we observed among terminators were not statistically significant (two-way ANOVA, $p > 0.05$) (Figure 1c, Figure S5). Taken together, these data suggest that varying the terminator is a valuable way to fine-tune gene expression, particularly when certain regulatory characteristics of the promoter (*e.g.*, responsiveness to growth phase or gut conditions) must be maintained.

**The *S. boulardii* Genome Can Be Efficiently Modified by CRISPR-Cas12a Genome Editing.** Genomic integration of synthetic constructs can sidestep undesirable issues associated with the use of plasmids in the gut. These issues include plasmid instability, spreading to other microbes, collateral damage to the microbiota if antimicrobials are used for plasmid selection, and the increased metabolic burden of maintaining multicopy plasmids. Further, genome integration increases the uniformity of gene expression throughout the engineered cell population.[54] However, different genomic regions are known to support varying levels of synthetic construct expression, potentially due to nucleosome positioning,[55] and integrating material into the genome can be difficult for diploid organisms.[56]

To characterize and overcome inefficiencies associated with genome integration, we compared three different editing


https://doi.org/10.1021/acssynbio.0c00562
ACS Synth. Biol. 2021, 10, 1039−1052

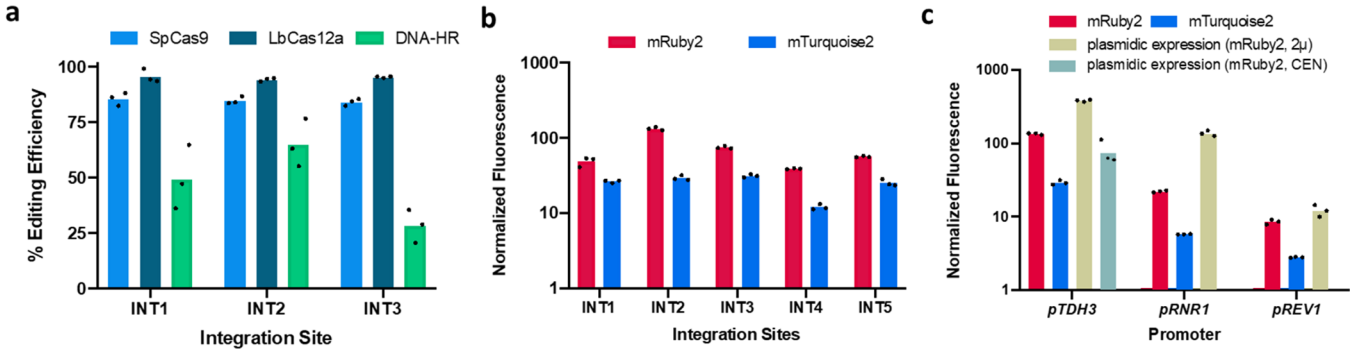


**Figure 2.** *S. boulardii* genomic location impacts gene expression, and comparison of genome editing techniques. (a) Editing efficiency at 3 different loci using 3 different methods: CRISPR/SpCas9 (SpCas9), CRISPR/LbCas12a (LbCas12a), and unassisted linear dsDNA integration (dsDNA integration). Three different guides were used for both SpCas9 and LbCas12a for each site. Each dot represents one guide. Three replicate cultures were transformed with the DNA repair template to measure the efficiency of genome editing in *Sb via* dsDNA integration. Table S4 shows the number of colonies screen for each method. (b) Effect of chromosomal locus on the expression of the fluorescent genes mRuby2 and mTurqouise2. Each dot represents one biological replicate. (c) The effects of promoter (strong, medium, or weak) on gene expression at the same chromosomal locus (INT2). Each dot represents one biological replicate.

methods in the diploid *Sb*: unassisted linear dsDNA integration (dsDNA integration) and genome editing assisted with the CRISPR nucleases SpCas9 or LbCas12a. We tested the ability of these methods to integrate a linear expression cassette containing *mTurquoise2* in three different loci (INT1, 2, and 3). In the case of unassisted dsDNA integration, 4/12 transformants did not contain the expected *mTurquoise2* insertion, while 7/12 colonies yielded multiple fragments after colony PCR (Figure S6). Sequencing revealed that the larger fragment corresponded to the desired integration, while the shorter fragment corresponded to the native genomic locus. This result is likely due to the fact that the *Sb* genome is diploid, and that integration of one copy is sufficient to confer uracil prototrophy. Therefore, we tested whether CRISPR/Cas systems could achieve higher genome editing efficiency. We reasoned that since CRISPR/Cas systems enhance the proportion of double-stranded breaks in all copies of the targeted sequence, editing of all chromosomal copies would be a preferred survival strategy. Three sgRNAs for SpCas9 and three gRNAs for LbCas12a were designed for each integration site. Targeted loci were followed by a 5′-NGG-3′ protospacer adjacent motif (PAM) for SpCas9 and preceded by a 5′-TTTV-3′ PAM (V = A, C, G) for LbCas12a. Figure S7 shows the plasmid designs we used for CRISPR-based editing. Table S2 shows integration locations (INT1−INT5) in *Sb*'s genome. These integration sites were chosen based on high expression levels from previously characterized chromosomal sites in *Sc*,[57,58] and Table S3 shows the guide RNA sequences we used.

We tested the editing efficiency at each integration site (using one guide RNA per experiment) as above for unassisted linear DNA integration. Table S4 shows the number of fluorescent colonies we observed for each editing method. Genome editing efficiencies were determined by the number of fluorescent colonies divided by the number of all transformants on a transformation plate as previously described.[59] Colony PCR of random transformants from each experiment revealed a single band corresponding to either the edited or the unedited version of the locus (Figure S8). Altogether, we were able to generate genome integrants in *Sb* with 82−88% efficiency using SpCas9 and 93−99% efficiency using LbCas12a (Figure 2a, Table S4). This high efficiency indicates that LbCas12a is an excellent candidate for the integration of libraries into the *Sb* genome in future work. Finally, these experiments indicate that the many CRISPR-Cas tools developed for engineering *Sc* may be easily extended to *Sb*.

**Integration Locus Has a Minor Effect on Gene Expression Relative to Promoter Choice.** To determine the extent of locus-dependent effects on gene expression in *Sb*, we integrated expression constructs for *mRuby2* or *mTurquoise2* into five different locations in the *Sb* genome (Table S2) using LbCas12a. These genes were regulated by *pTDH3* and *tTDH1*, and constructs contained *URA3* to select for edited strains (Figure S7b). The *mRuby2* and *mTurquoise2* fluorescent proteins are sequence-divergent, with only 30% amino acid identity. These two proteins therefore enabled a cursory view into the generalizability of expression patterns across genes. Across integration sites, the expression of *mRuby2* and *mTurquoise2* varied 3.4-fold and 2.6-fold, respectively (Figure 2b, Figure S9). INT4 supported the lowest expression for both genes, while INT2 supported the highest expression levels for *mRuby2* and INT3 supported the highest expression level for *mTurquoise2*. We next asked whether differences in promoter strength observed in the plasmid-based system would be similar for genomically integrated constructs. We therefore expressed *mRuby2* and *mTurquoise2* from two additional promoters in INT2: *pRNR1* and *pREV1*. Intriguingly, genomic *mRuby2* expression varied by 5.9-fold between *pTDH3* and *pRNR1*, compared with 2.8-fold for the same constructs on a *2μ* plasmid. Conversely, genomic *mRuby2* expression varied by 15.3-fold between *pTDH3* and *pREV1*, compared to 31.2-fold for the same constructs on a *2μ* plasmid (Figure 2c). This could indicate that gene expression from high-copy plasmids saturates at high promoter strengths, or that promoter strength varies with copy number due to transcription factor dilution. Additionally, we found that *mRuby2* and *mTurquoise2* fluorescence values were highly correlated ($R^2$ = 0.9945, Figure S9c). This correlation, measured for two genes with 30% amino acid identity, indicates that the expression patterns we observed among the promoters we tested may extend to other genes. Together, this work identifies regions of the *Sb* genome enabling high-level expression of synthetic constructs. Further, these data show that the impact of integration locus on gene expression is relatively small in *Sb* compared to that of the promoter.

***S. boulardii* Facilitates High-Throughput Metabolic Engineering through *in Vivo* Combinatorial Assembly**


https://doi.org/10.1021/acssynbio.0c00562
ACS Synth. Biol. 2021, 10, 1039−1052

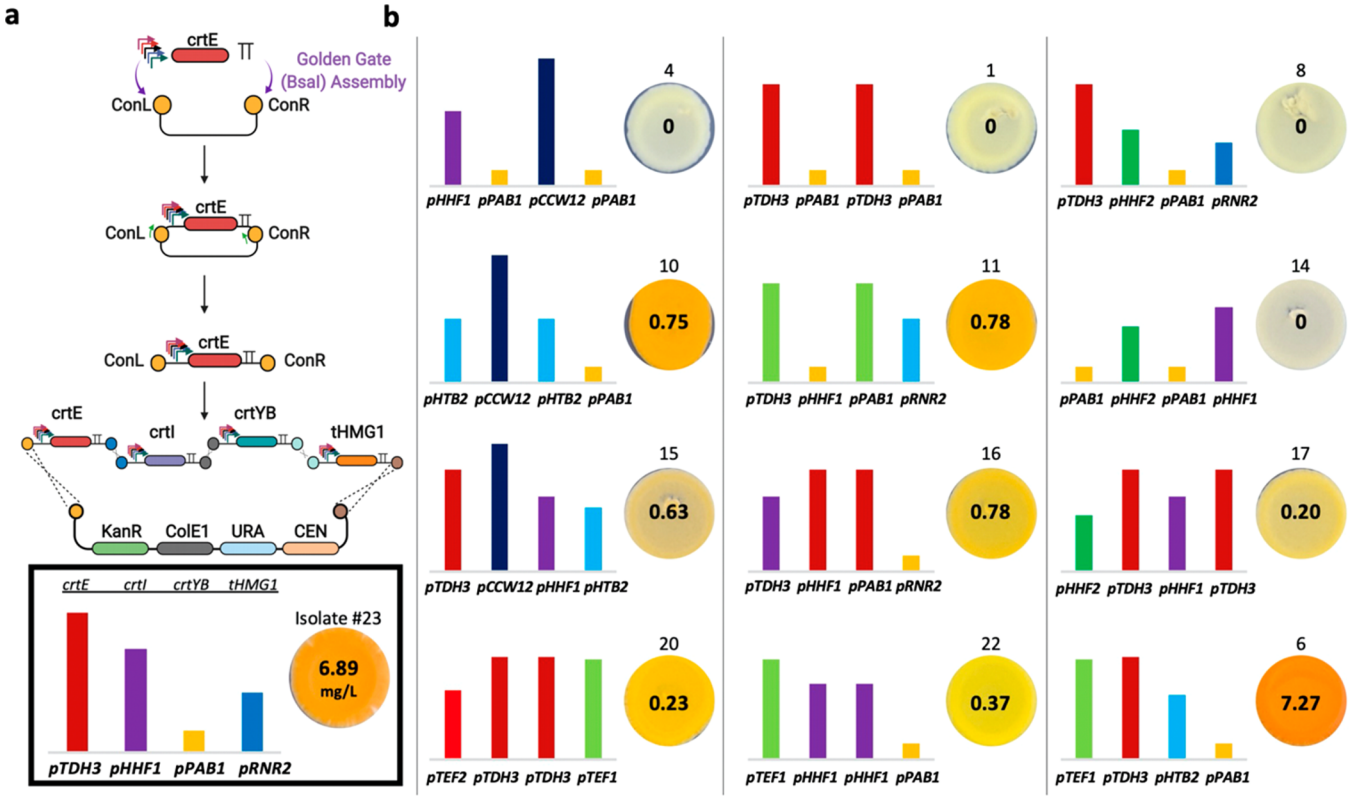


**Figure 3.** Combinatorial assembly of the $\beta$-carotene pathway in *Saccharomyces boulardii*. (a) Overview of assembly steps. Genes in the $\beta$-carotene pathway were randomly cloned behind 9 promoters (*pTDH3, pCCW12, pHHF2, pTEF1, pTEF2, pHHF1, pHTB2, pPAB1, pRNR2*). *tSSA1, tADH1, tTDH1,* and *tENO1* terminators were cloned behind *crtE, crtI, crttYB-2,* and *tHMG1*, respectively. The backbone plasmid contains Type1 and Type2 YTK connectors to enable *in vivo Sb* assembly. Promoter-gene-terminator regions between the two connectors were amplified and the PCR products were transformed to *Sb* for pathway assembly into a linear backbone *via* connector-assisted homologous recombination, as described in the Methods section. (b) Sequencing and $\beta$-carotene quantification of isolates from yeast transformation plates (Figure S10b). Thirteen out of 28 isolates (Figure S10d) were selected to proceed with sequencing and $\beta$-carotene quantification based on stability of colony color after 3 serial passages. Promoter sequences were confirmed by Sanger sequencing with reverse primer binding on the gene of interest (backbone for *tHMG1*) and forward primer binding on the terminator of the previous gene (backbone for *crtE*). Quantification of $\beta$-carotene was done by high-performance liquid chromatography (HPLC) as described in the Methods section. The spot images were taken from Figure S10d. The number above the spots corresponds to the spot number on Figure S10d. The bar heights represent the normalized fluorescence values in linear scale for each promoter according to promoter characterization work (Figure 1a). The numbers in the center of the spots corresponds to average $\beta$-carotene produced by 3 biological replicates of each isolate in one liter of saturated yeast culture.

**of Multienzyme Pathways.** Having found that *Sb* could support genome integration *via* homologous recombination, we asked if recombination efficiencies were sufficient for *in vivo* assembly of biosynthetic pathways. In *Sc*, combinatorial *in vivo* assembly enables rapid optimization of metabolic pathways.[60−62] Large scale assembly of metabolic pathways directly in *Sb* would simplify strain development and reveal the potential for *Sb* as a host for small molecule production. For this demonstration, we focused on the $\beta$-carotene and violacein synthesis pathways because these compounds provide a direct colorimetric readout of assembly efficacy (Figures S10a and S10b). While $\beta$-carotene is a precursor to the essential vitamin A and violacein has been explored as an anticancer drug,[63] our focus was on establishing the first *in situ* production titers from *Sb* rather than developing a therapeutic. The $\beta$-carotene pathway was also interesting because the optimal expression levels for several genes are not obvious from the biosynthetic reaction map.[64] In particular, *HMG1* diverts flux from cellular acetyl-CoA pools into the $\beta$-carotene pathway, thereby reducing the amount of acetyl-CoA available for other processes. *crtYB* can convert lycopene into the desired product $\beta$-carotene, but can also convert neurosporene (a precursor to lycopene) into the side product 7,8-dihydro-$\beta$-carotene ($\beta$-zeacarotene). *crtI* operates on several pathway intermediates, including phytoene, $\zeta$-carotene, and neurosporene.[65] We therefore exploited *Sb*'s homologous recombination machinery to rapidly construct and reveal efficient $\beta$-carotene and violacein synthesis pathways.

We started from our characterized promoter, coding sequence (CDS), and terminator parts and assembled pathways directly in yeast with minimal subcloning (Figure 3a). Our assembly strategy involved two steps. First, golden gate assembly was used to assemble a 9-member promoter library for each gene. These gene-level libraries were then PCR-amplified directly from the Golden Gate reaction mixture and contained homology arms to facilitate *in vivo* assembly. Purified amplicons were transformed into *Sb*, where flanking sequences directed homology-dependent assembly of the final pathway with one variant of each transcriptional unit. Figures S10c and S10d show spotted cultures of 28 members from the $\beta$-carotene library and 24 members from the violacein library. Colony sequencing revealed that each strain harbored a plasmid containing the expected pathway topology, with each


https://doi.org/10.1021/acssynbio.0c00562
ACS Synth. Biol. 2021, 10, 1039−1052

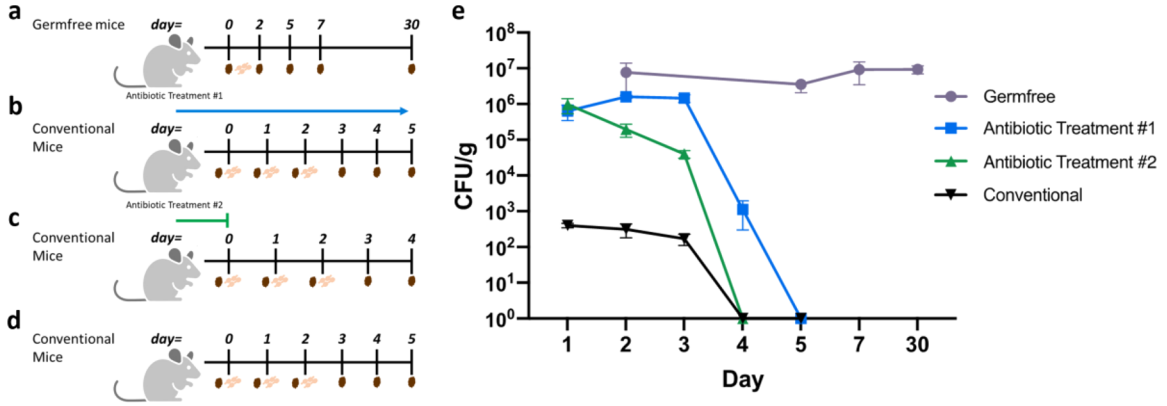


**Figure 4.** Microbial competition reduces *S. boulardii*'s residence time in mice. (a) Germ-free mice were gavaged with wild-type *Sb* (pink dots) on day 0. (b) Conventional mice were treated with 1 mg/mL penicillin and 2 mg/mL streptomycin in drinking water for 4 days prior to 3 *Sb::NatR* (pink dots) treatments every 24 h (antibiotics were replenished every 4 days). (c) Conventional mice were treated with 1 mg/mL penicillin and 2 mg/mL streptomycin in drinking water for 4 days prior to 3 *Sb::NatR* (pink dots) treatments every 24 h (antibiotic treatment was stopped on day 0). (d) Conventional mice were treated with 3 *Sb::NatR* (pink dots) gavages every 24 h. (e) Fecal carriage of *Sb* in the three mouse models. Fecal samples were collected as shown in the timelines and plated on YPD media for the gnotobiotic model or YPD containing antibiotics for the conventional models. Error bars indicate the standard deviation observed among 4 germ-free mice, 3 conventional mice treated with antibiotic treatment #1, and 3 conventional mice treated with antibiotic treatment #2. In all mouse models, feces (brown dots) were collected prior to *Sb* gavage during days when both occurred.

gene driven by one of the 9 selected promoters and the desired terminator.

We next identified strains exhibiting qualitatively stable coloration over three rounds of growth of solid media. Thirteen out of 28 $\beta$-carotene-producing strains and 8 out of 24 violacein-producing strains exhibited stable production levels. Due to its relevance as a vitamin precursor, we determined the identity of the promoters driving each gene in the $\beta$-carotene pathway and quantified the amount of $\beta$-carotene produced by each strain to understand how different combinations of promoters regulate biomolecule production (Figure 3b and Figure S11). The highest $\beta$-carotene titer we achieved was 7.27 mg/L from SPC554, corresponding to 0.036 pg/cell. Interestingly, we found that strains with the highest qualitative color intensity and $\beta$-carotene titer did not harbor strong promoters for all genes. In fact, many high producers contained moderate or low-strength promoters in at least one of their genes, supporting the utility of a diverse panel of gene expression regulators for production of small molecules in high titers. Additionally, we observed cases where multiple genes in a high-producing strain were driven by the same promoter. This suggested that metabolic burden in these strains was not high enough to select for the emergence of nonproducers *via* homologous recombination. Our results reveal that, as in *Sc*, large combinatorial pathway libraries can be easily generated in *Sb*, enabling rapid optimization of small molecule biosynthesis pathways.

**The Mouse Microbiota Restricts *S. boulardii* Colonization.** Host immunity, intestinal peristalsis, intermicrobial competition, and nutrient availability shape the residence time of microbes in the gut. To parse this complexity, gnotobiotic mouse models are attractive to explore the behavior of microbes in defined gut ecologies. While the residence times of *Sb* has been measured in humans, rats, and antibiotic-treated mice, its residence time in other mouse models was unknown.[37,39,66,67] Therefore, we first measured *Sb*'s residence time in the germ-free mouse gut by delivering *Sb* ($10^8$, $10^7$, or $10^6$ colony-forming units) to germ-free mice *via* oral gavage (Figure S12). No deleterious effects on mouse health were apparent during the experiment. While all dosages yielded similar fecal loads of *Sb* through day 5 ($3 \times 10^6$ CFU/g feces), we found that when mice were provided at least $10^8$ CFUs, consistent fecal loads of $10^7$ CFU/g *Sb* were maintained for over 30 days. On the other hand, mice gavaged with $10^6$ and $10^7$ CFUs showed 3-fold lower fecal titers starting on day 7. Thus, the initial dose of *Sb* impacts its fecal titer and residence time in germ-free mice. Furthermore, in the absence of microbial competitors, *Sb* is capable of long-term (>30 days) colonization of the gut.

We next asked whether the presence of microbial competitors would modulate the gut residence time of *Sb*. To answer this, we turned to conventionally raised mice, with and without simultaneous antibiotic treatment to lower colonization resistance.[68] In these experiments, we were initially unable to track *Sb* titers *via* plating because other commensal fungi outgrew *Sb* on YPD plates containing 0.125 mg/mL penicillin and 0.25 mg/mL streptomycin. Therefore, we hypothesized that integration of an antifungal resistance gene into the *Sb* genome would allow easier identification *via* plating on media containing antifungals. On the basis of the observed minimum inhibitory concentrations (MICs) of various antifungals against *Sb* (Figure S13), we integrated the nourseothricin resistance gene (*NatR*) into the *Sb* genome (INT1). We found that *NatR*-containing *Sb* was the only microbe from mouse feces able to grow on YPD plates containing 50 $\mu$g/mL nourseothricin, 0.125 mg/mL penicillin, and 0.25 mg/mL streptomycin (data not shown). We then provided conventional mice with 1 mg/mL penicillin and 2 mg/mL streptomycin in their drinking water for 4 days, after which $10^8$ CFU of *Sb* was delivered once per day for 3 days. Antibiotics were maintained over the course of the experiment (Treatment 1, Figure 4b). We observed ~$10^6$ CFU *Sb* per gram feces during and 1 day after the last gavage, after which *Sb* titers fell to undetectable levels 3 days after the last gavage (Figure 4e). When antibiotic treatment ceased upon *Sb* delivery (Treatment 2, Figure 4c), its residence time was shortened, dropping to undetectable levels within 48 h after the last gavage. We then provided the same dosage of *Sb* to


https://doi.org/10.1021/acssynbio.0c00562
ACS Synth. Biol. 2021, 10, 1039−1052

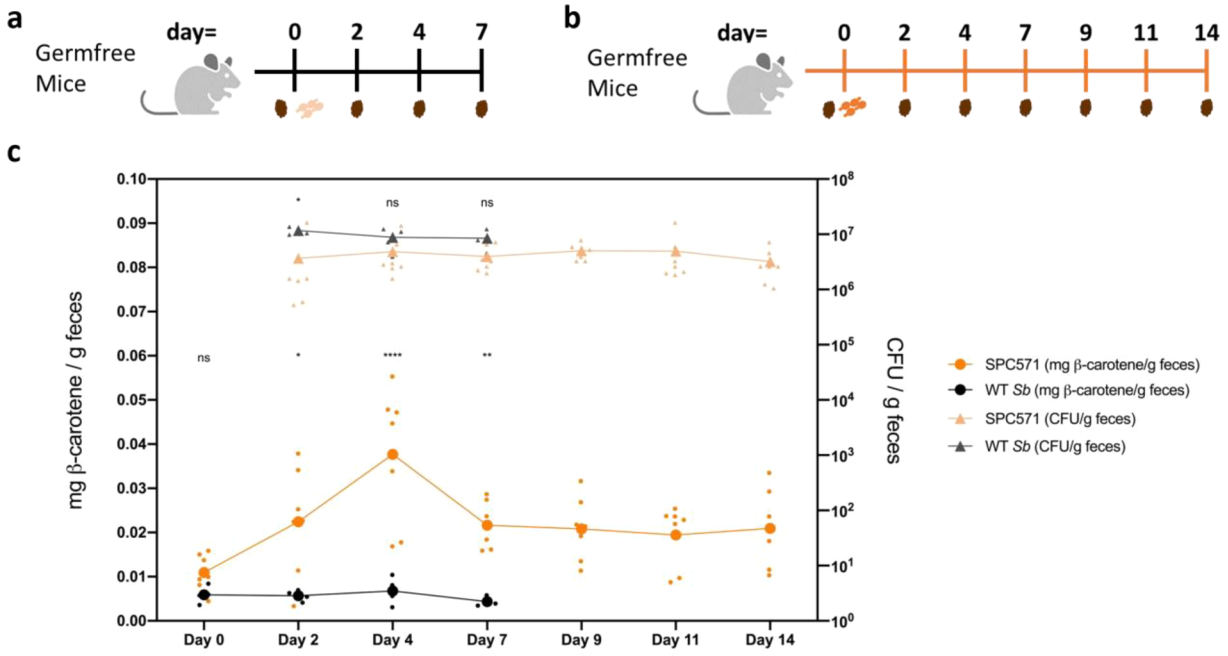


**Figure 5.** Engineered *S. boulardii* can produce β-carotene in the mammalian gut. (a) Germ-free mice were gavaged with wild-type (WT) *Sb* on day 0 and followed for 7 days. (b) Germ-free mice were gavaged with β-carotene-producing *Sb* (SPC571) on day 0 and followed for 14 days. (c) Fecal carriage of WT *Sb* (gray line) and SPC571 (beige line) in feces and β-carotene load (mg) in feces of mice gavaged with WT *Sb* (black line) and SPC571 (orange line). Smaller circles and triangles represent the data obtained from individual mice (for WT *Sb* $n = 4$, for SPC571 $n = 7$). The mean fecal levels of *Sb* and β-carotene are presented as large triangles and dots, respectively. One-way ANOVA with Sidak's multiple comparisons test were conducted between WT and SPC571 treatment groups. (ns $P > 0.05$, *$P < 0.05$ **$P < 0.005$, ***$P < 0.0005$, ****$P < 0.0001$)

conventional mice in the absence of antibiotic treatment (Figure 4d). In this case, the carriage of *Sb* was much lower—only reaching ~$10^3$ CFU/g 24 h after each gavage. These results are in line with previous *Sb* colonization studies performed in mice colonized by a human microbiota[67] and indicate that competitive microbial growth reduces the residence time of *Sb* in the mouse gut. In these contexts, *Sb*-mediated drug delivery will only occur during and for several days after probiotic administration, thereby minimizing dosage outside of desired therapeutic time scales.

Studying colonization profiles in the gut provides insights into the behavior of the host and the introduced microbe(s). While further work is necessary to fully elucidate the effects of *Sb* colonization on both mice and *Sb*, our work presents an overview for when each mouse model can be used. Specifically, germ-free mice are appropriate for "proof-of-principle" testing of biomolecule production in the gut environment, since colonization levels were the highest in this setting. On the other hand, conventional and antibiotic treated mice are appropriate for testing the impact of transience on biomolecule production, and for testing the effects of *Sb* on the native microbiota. Elucidating the interactions between *Sb* and individual microbiota members *via* gnotobiotic experiments is of significant future interest.

**Engineered *S. boulardii* Can Produce β-Carotene in the Mouse Gut.** Having identified the *Sb* strains that produce high-titers of β-carotene in culture, we asked whether *Sb* can produce β-carotene in the gut, how much β-carotene it can produce, and whether β-carotene-producing yeast exhibits a colonization defect. We chose SPC571 (isolate #23), a strong β-carotene producer (Figure 3b), to administer to 7 germ-free mice, since *Sb* attained its highest and most persistent colonization in this setting (Figure 4), and preliminary experiments in antibiotic-treated mice showed no detectable β-carotene increase (data not shown). As a control, we administered wild-type *Sb* to 4 germ-free mice. $10^8$ cells were administered to both groups (Figure 5a,b). For SPC571, the average fecal load of *Sb* was consistent over the course of the 14-day experiment ($5 \times 10^6$ CFU/g feces) (Figure 5c). For wild-type, the average fecal load was $10^7$ CFU/g (Figure 5c), which is similar to what we observed during the previous colonization experiment (Figure 4d). While colonization levels for wild-type and engineered *Sb* were different during the first 48 h postgavage ($p < 0.05$), longer-term colonization profiles were similar ($p > 0.05$). These data indicate that β-carotene-producing *Sb* exhibited a similar ability to colonize germ-free mice, as compared to wild-type *Sb*.

Knowing that β-carotene-producing *Sb* could successfully colonize the germ-free mouse gut, we quantified the amount of β-carotene present in feces from both groups. We saw that colonization by wild-type *Sb* did not change fecal β-carotene levels from baseline dietary levels (~5 μg/g feces) (Figure 5c). However, after colonization by SPC571, fecal β-carotene levels rose to a maximum of 37 μg/g feces on day 4, corresponding to an increase of 27 μg/g feces above day 0 levels. β-carotene levels in these mice remained higher than precolonization levels throughout the experiment (one-way ANOVA with Sidak's multiple comparisons test, min $p$-value <0.0001). Additionally, fecal β-carotene from mice colonized by SPC571 was significantly higher than from mice colonized by wild-type on the same day (one-way ANOVA with Sidak's multiple comparisons test, max $p$-value <0.05) (Figure 5c).

Integrating production and colonization data, 5.98 pg of β-carotene per viable *Sb* cell was produced in the large intestine, 174-fold higher than was obtained for the same strain in culture (Supplementary Text S1). While the cause of this


https://doi.org/10.1021/acssynbio.0c00562
ACS Synth. Biol. 2021, 10, 1039−1052

discrepancy is unknown, one possibility is that cell death is occurring within the gut. Additionally, this increase could be due to environmental factors (nutrients, pH levels, slow replication rates) which collectively increase the per-cell titers of β-carotene in the gut. Integrating the additional β-carotene produced by SPC571 over the entire experiment, approximately 194.4 μg β-carotene was synthesized *in situ* by engineered *Sb*, 56-fold more than the amount of β-carotene present in the *Sb* cells gavaged on Day 0 (3.5 μg) (Supplementary Text S2). This indicates that *in situ* biosynthesis of β-carotene occurred during the experiment. Our results reveal a surprising discrepancy between *Sb*'s *in vitro* small molecule titers and its performance *in vitro*, indicating that more realistic *in vitro* models could enable rapid prototyping of engineered *Sb* prior to animal experiments.[69−74]

On average, 14.14 μg β-carotene was produced per gram of feces. Extrapolating this value to the average fecal mass produced per day in humans (128 g)[75] yields 1.8 mg of β-carotene, or 150 μg of retinoic acid equivalent.[76] While the recommended intake of retinoic acid is 900 μg and 700 μg in men and women, respectively,[76] we expect that the presence of a microbiota and the substantially longer gut residence time will cause β-carotene production in humans to be different from that measured here in germ-free mice. Furthermore, the bioavailability of β-carotene produced by probiotic yeast in the large intestine is likely to be low, as β-carotene absorption occurs in the small intestine. Therefore, release of β-carotene from the yeast cell, and conversion of β-carotene to immunomodulatory carotenoid derivatives,[77,78] are interesting areas of future study.

Interestingly, all yeast isolated from SPC571-colonized mice throughout the experiment exhibited a striking orange color, even though colonies were isolated on nonselective media. We passaged several of these isolates through three rounds of restreaking on solid selective media, and their orange color was maintained. This indicates that *Sb* successfully maintained the *URA3*-marked plasmid encoding the β-carotene pathway, presumably in the absence of selective pressure for plasmid maintenance in the gut environment. Taken together, these data show that *Sb* is metabolically active and can be engineered to synthesize β-carotene, a precursor to an essential vitamin, over 14 days in the mammalian gut.

## CONCLUSION

The gut and the microbes that live within it play a major role in health, and as such are promising targets for small molecule or biologic drugs. Unfortunately, delivering drugs to the gut remains challenging due to the digestive action of the host. Due to its probiotic properties and similarity to the biomanufacturing workhorse *Sc*, we established a synthetic toolkit for *Sb* engineering and applied this toolkit to produce a vitamin precursor in the mammalian gut. We first demonstrated tunability of gene expression over 2 orders of magnitude using plasmid-based constructs derived from *Sc*. We next established >95% efficient genome editing using LbCas12a and revealed up to 3.4-fold variation in gene expression depending on the genomic integration site. We further harnessed *Sb*'s high rates of homologous recombination to combinatorially assemble pathways for vitamin precursor (β-carotene) and drug (violacein) production, revealing designs that enable up to 7.27 mg/L β-carotene in shake-flask culture. We next determined *Sb*'s ability to colonize germ-free and antibiotic-treated mice and found that microbial competitors significantly reduce *Sb*'s gut residence time. Finally, we found that β-carotene-producing yeast can colonize germ-free mice over 14 days and continuously produce β-carotene (194.4 μg total). These results indicate that *Sb* is a promising probiotic chassis, and point to several areas of future research to further improve its delivery properties, including gut residence time and ability to secrete biomolecules and proteins. We are currently investigating the ability of *Sb* to release β-carotene to its surroundings *via* cell lysis or export, as has been demonstrated in related yeast species.[79,80] Taken together, these results expand our ability to tune biomolecule production in the promising probiotic eukaryote *Sb*.

## METHODS

**Strains and Culture Media.** *Escherichia coli* Top10, NEB 5α and NEB 10β were used for plasmid construction and maintenance. *E. coli* cells were grown in lysogeny broth (LB) (5g/L yeast extract, 10 g/L tryptone, 10 g/L NaCl) at 37 °C supplemented with ampicillin (100 μg/mL), kanamycin (50 μg/mL) or chloramphenicol (50 μg/mL). *Saccharomyces boulardii* ATCC-MYA796 was used for antifungal marker and origin of replication characterization. *Saccharomyces boulardii* Δ*URA3*, provided by Yong-Su Jin, was used for auxotrophic marker, origin of replication, promoter, and terminator characterization, as well as genome editing and metabolic pathway assembly. *Saccharomyces boulardii* Δ*TRP1* and Δ*HIS3* strains from the Jin Lab were used for auxotrophic marker and origin of replication characterization. Promoter and terminator characterization experiments were conducted in synthetic media containing 0.67% (w/v) Yeast Nitrogen Base Without Amino Acids (Sigma-Aldrich), 2% Glucose (Fisher Scientific), 1.92g/L Yeast Synthetic Media Drop-Out Mix without Uracil (Sigma-Aldrich). For auxotrophic marker characterization, synthetic media with 0.67% (w/v) Yeast Nitrogen Base Without Amino Acids (Sigma-Aldrich), 2% Glucose (Fisher Scientific), and 1.92% Yeast Synthetic Media Drop-Out Mix without the appropriate nutrient (histidine, tryptophan, or uracil) (Sigma-Aldrich) was used. Antifungal marker characterization experiments were conducted in yeast extract-peptone-dextrose medium (50 g/L YPD broth (Sigma-Aldrich)) supplemented with various concentrations (50 μg/mL, 100 μg/mL and 200 μg/mL) of Geneticin (G418), zeocin, nourseothricin and hygromycin.

**Plasmid Construction and Cloning.** A synthetic toolkit (MoClo-YTK) containing yeast parts were gifts from the Dueber Lab (Addgene #1000000061). Characterization plasmids consisted of 8 parts: 2 connectors, promoter, coding sequence, terminator, yeast marker, yeast origin, and *E. coli* marker and origin. Each of these plasmids were assembled according to Deuber lab YTK protocols *via* Golden Gate cloning.[81] The Golden Gate reaction mixture, for all plasmids except those containing β-carotene or violacein pathways, was prepared as follows: 0.5 μL of 40 nM of each YTK plasmid (20 fmol), 0.5 μL T7 Ligase (NEB) or 0.5 μL T4 Ligase (NEB), 1 μL T4 Ligase Buffer (NEB) and 0.5 μL BsaI (10 000 U/mL, NEB) and water to bring the final volume to 10 μL. The Golden Gate assembly protocol was performed on a thermocycler with the following program: 30 cycles of digestion (42 °C for 2 min) and ligation (16 °C for 5 min), followed by a final digestion (60 °C for 10 min) and heat inactivation (80 °C for 10 min).

**Yeast Competent Cells and Transformations.** We optimized the yeast competent cell preparation and trans-


https://doi.org/10.1021/acssynbio.0c00562
ACS Synth. Biol. 2021, 10, 1039−1052

formation protocol from Gietz et. al for *Saccharomyces boulardii*.[82,83] For the characterization experiments, we used frozen competent cells, whereas for the genome editing experiments we used unfrozen competent cells prepared on the same day.[82,83] To prepare competent cells, yeast colonies were inoculated into 1 mL YPD and incubated in a shaking incubator overnight at 37 °C, 250 rpm. This culture was diluted into fresh 50 mL YPD (approximately $OD_{600}$ = 0.25), and grown for 6−8 h until $OD_{600}$ = 1. The culture was centrifuged at 3000*g* for 5 min at room temperature to pellet the cells. After decanting the media, the pellet was resuspended in 25 mL of sterile water, and then pelleted at 3000*g* for 5 min. This pellet was resuspended in 1 mL of sterile water. The cells were then pelleted at 10 000*g* for 1 min and water was discarded. The cells were then resuspended in 500 μL of frozen competent cell solution consisting of 2.5% (v/v) glycerol (Sigma-Aldrich) and 5% (v/v) DMSO (Thermo-Fisher). 50 μL of this suspension was aliquoted into 1.5 mL microcentrifuge tubes and stored in −80 °C. For transformations, frozen cells were thawed at 37 °C for 1 min. Then, the cells were pelleted by centrifugation at 3000*g* for 2 min, after which the supernatant was removed. Then, solutions were added in the following order; 260 μL 50% PEG3350 (Fisher Scientific), 36 μL 1 M Lithium Acetate (Sigma-Aldrich), 50 μL of 2 mg/mL single-stranded salmon sperm DNA (Invitrogen, 15632011), 0.1−10 μg DNA, and water to bring the final volume to 360 μL. Ten mg/mL double-stranded salmon sperm DNA from the supplier was diluted to 2 mg/mL and heat treated at 95 °C for 5 min to denature the double-stranded DNA. The pellet was resuspended in the transformation mix by gently mixing with a pipet tip. This transformation mix was incubated at 42 °C for 1 h. This mixture was then centrifuged at 3000*g* for 1 min and the supernatant was discarded. The cell pellet was resuspended in 1 mL YPD by gently pipetting up and down and this tube was incubated at 37 °C for 1 h. Then, the cell suspension was centrifuged for 1 min at 3000*g*, resuspended in 25 μL sterile water, and plated on an appropriate growth media.

**_S. boulardii_ Colony PCR.** Since *Sb* has a thicker cell wall than *Sc*, we developed a new method to perform colony PCR on *Sb*. Colonies were picked into 25 μL 20 mM sodium hydroxide and incubated at 98 °C for 80 min. Then we centrifuged these reactions at max speed (Mini Microcentrifuge Sargent-Welch) for 10 min and started a 25 μL PCR reaction with 2 μL of this reaction as a template. Otherwise, PCR reactions were performed according to the supplier's instructions.

**Flow Cytometry.** Constructs were inoculated from −80 °C freezer stocks into 750 μL of appropriate media in 96-deep-well plates (VWR International) and incubated at 37 °C for 36 h with shaking at 250 rpm. After 36 h, the cultures were diluted 1:100 in 200 μL of fresh media in 96-well-plates (Costar) and were grown for ∼8−10 h at 37 °C. Once the cultures reached $OD_{600}$ values between 0.1 and 0.4, flow cytometry was performed using a MACSQuant VYB (Miltenyi Biotec). Cells containing empty vector were used as a control. The voltage of the channels was adjusted in order to tune the gain of the detectors. The voltage values applied to FSC, SSC, Y1 (PE-A, excitation:561, emission: 586/15 nm), V1 (CFP-VioBlue, excitation: 405 nm, emission: 450/50 nm) and B1 (GFP_FITC, excitation: 488 nm, emission: 425/50 nm) channels/filters were 326V, 290V, 396V, 324V, and 265V respectively. No gating was performed. Flow cytometry data analysis was conducted on the FlowJo program (FlowJo LLC). The mean fluorescence values obtained from the flow cytometry for each transcriptional construct were then normalized to background fluorescence (*i.e.*, the cells with an empty vector).

**Mouse Experiments.** All mouse experiments were approved by the NC State University Institutional Animal Care and Use Committee (IACUC).

**Germ-Free Mice.** *Colonization Experiments (Figure 4).* 6−10 week old male and female germ-free C57BL/6 mice were monocolonized by wild type *S. boulardii*. Two mice (males) were gavaged with $10^6$ colony forming units in 100 μL PBS, 8 mice (6 females and 2 males) were gavaged with $10^7$ and 4 mice (2 females and 2 males) were gavaged with $10^8$ *Sb* cells on day 1 and fecal samples were collected on days 2, 5, and 7. Fecal samples from mice housing the $10^8$ inoculum were also collected on day 30.

*β-Carotene Production Experiment Negative Control (Figure 5).* 20−28 week old male germ-free C57BL/6 mice were monocolonized by wild type *Sb*. All 4 mice were gavaged with $10^8$ *Sb* cells on day 0 and fecal samples were collected on days 0 (prior to gavaging with *Sb*) 2, 4 and 7.

*β-Carotene Production Experiment (Figure 5).* 12−14 week old male germ-free C57BL/6 mice were monocolonized by recombinant *Sb* capable of synthesizing β-carotene. All 7 mice were gavaged with $10^8$ β-carotene producing *Sb* cells on day 0. Prior to gavaging on day 0, fecal samples were collected from all mice to capture baseline β-carotene levels. After the gavage took place, fecal samples were collected on days 2, 4, 7, 9, 11, and 14. On day 14 after the fecal sample collection, the mice were sacrificed and the cecum and the colon contents were collected.

*Stool Cultures.* Two pieces of stool were added to preweighed 1.5 mL microcentrifuge tubes and then weighed again to determine the fecal mass. Cecum and colon contents were collected in preweighed 5 mL reagent tubes and then weighed again to determine the intestinal content mass. Fecal and intestinal matter was then resuspended in 1 mL PBS per 100 mg feces/intestinal matter. Fecal and intestinal matter suspensions from monocolonized mice were placed on solid YPD media. Plates were incubated in 37 °C for 2−3 days until the colonies appeared.

**Conventional Mice.** Six-week old female C57BL/6J mice were obtained from Jackson Laboratories and hosted at the NCSU Biological Resources Facility (BRF) for 3−4 days before experiments. Mice were housed in groups of three and their cages were changed before treatment with antibiotics (if necessary) and before treatment with *Sb::NatR* or water. Antibiotic-treated mice were provided 1 mg/mL penicillin and 2 mg/mL streptomycin in their drinking water for 4 days starting on day −3. On day 1, drinking water was either replenished with antibiotic solution or changed to fresh water. Mice were then gavaged with $10^8$ CFU *Sb* or water once every 24 h for 3 days. Fecal samples were collected every 24 h from day 1 to day 5.

*Stool Cultures.* 1−2 pieces of stool were collected in preweighed 1.5 mL centrifuge tubes and then weighed again to determine fecal mass. Fecal matter was then resuspended in 1 mL PBS per 100 mg feces. Fecal suspensions from monocolonized mice were placed on solid YPD media, while fecal suspensions from conventional mice treated with antibiotics were plated on YPD media containing 50 μg/mL


https://doi.org/10.1021/acssynbio.0c00562
ACS Synth. Biol. 2021, 10, 1039−1052

nourseothricin and 0.25 μg/mL streptomycin. Plates were sealed with parafilm and incubated at 37 °C for 2−3 days.

**Genome Editing.** Integration plasmids contained *URA3* to aid selection and contained homology arms between 350 to 900 base pairs in length as shown in Figure S7. For DNA homologous recombination without DSB (dsDNA integration), 2 μg of linear donor DNA was transformed to $10^7$ *Sb* (*Sb* Δ*URA3*) competent cells prepared on the same day. For SpCas9, 2 μg of linear donor DNA and 1.5 μg of gRNA plasmids were transformed to $10^7$ freshly prepared chemical competent *Sb* Δ*URA3* cells containing SpCas9 plasmid. For LbCas12a, 2 μg of linear donor DNA and 1.5 μg of gRNA plasmids were transformed to $10^7$ freshly prepared chemical competent *Sb* Δ*URA3* cells containing LbCas12a plasmid.

Overnight cultures of *Sb* Δ*URA3* were grown in YPD only for Homologous Recombination, *Sb* Δ*URA3* containing the SpCas9 plasmid were grown in YPD + 100 μg/mL nourseothricin, and *Sb* Δ*URA3* containing the LbCas12a plasmid were grown in YPD + 200 μg/mL G418. Cultures were subinoculated to prewarmed YPD media with or without antifungals at an $OD_{600}$ of 0.25 and incubated at 37 °C with shaking at 250 rpm until cultures reached an $OD_{600}$ of 0.9−1.0. Cultures were then centrifuged at 3000*g* for 5 min. Cells were then washed twice with 0.5 and 0.1 volumes of sterile DI water at room temperature at 3000*g* for 5 min. The cells then were transformed according to the protocol described above, with the exception that heat shocked cells were spun down, resuspended in YPD, and incubated for 3 h at 37 °C. Transformed cells were then spread on Yeast Complete Synthetic Media (CSM) plates without uracil and with or without antibiotics. Plates were incubated at 37 °C for 2−4 days. Integration was verified with colony PCR.

**Combinatorial Pathway Assembly.** Prior to library assembly, promoter, gene, and terminator part plasmids were assembled into "entry vector" plasmids by BsmBI assembly. These plasmids had BsaI overhangs and follow the "Yeast golden gate toolkit" standard.[41] Backbones were assembled for subcloning of the transcriptional units. These backbones housed the appropriate homology arms for later final assembly of transcriptional units into a full pathway. BsaI assembly of transcriptional units into the matching backbone was completed by combining 10 fmol of each promoter part plasmid (to a total of 90 fmol) with 100 fmol of gene, terminator, and backbone plasmids. Reaction mixtures included 0.5 μL of BsaI-HF v2, 0.5 μL of T7 DNA Ligase, and 1 μL of T4 DNA ligase buffer (NEB), and underwent 50 cycles of golden gate assembly (2 min at 42 °C, 5 min at 16 °C), before a single 30 min final digestion at 60 °C, and 10 min of heat inactivation at 80 °C. Subsequently, we have noticed that final digestion steps of 5 min at 42 °C are more optimal for BsaI assembly.[81] Transcriptional units were amplified directly from the golden gate mixture using 1 μL of reaction mixture as template in 50 μL Q5 Hot-Start Master Mix reactions (NEB). PCR reactions were performed according to manufacturer's instructions and cleaned up using clean and concentrate kits (D4004-Zymo Research). 600 nM of each amplified transcriptional unit library was transformed using the lithium acetate protocol described above. Cells were recovered for 1 h in YPD prior to dividing the culture into 5 aliquots of 200 μL and plating on yeast nitrogen base plus amino acids without uracil (Sigma).

**Pathway Sequencing.** Random colonies were collected in 1.5 centrifuge tubes and resuspended in 1 mL of 10 mg/mL Lysing Enzymes from *Trichoderma harzianum* (L1412 Sigma). The cells were incubated in the lysing enzyme at 37 °C for 3 h and then the ZymoPURE Plasmid Miniprep (D4208T) was used to miniprep the plasmids. The Lysing Enzymes from *Trichoderma harzianum* help digest *Sb*'s cell wall and produce protoplasts that are easy to miniprep. 2 μL of the miniprep product was then used as a template to amplify the assembled region with primers complementary to the pathway genes or terminators, as the ordering of these was common to all constructs. The PCR product was then sent for Sanger sequencing (Genewiz, NJ, USA) to verify the promoters assigned for each gene.

**Antifungal Minimum Inhibitory Concentration Tests in *S. boulardii*.** Three biological replicates of *Sb* (ATCC-MYA796) were grown overnight in YPD media. Overnight cultures were subinoculated into YPD media with different antifungal concentrations ranging from 0 μg/mL to 200 μg/mL in a 96 well plate at starting $OD_{600}$ 0.02 and grown for 36 h in a plate reader (BioTek Synergy H1, Shake Mode: Double Orbital, Orbital Frequency: continuous shake 365 cpm, Interval: 10 min). Geneticin (G418), Nourseothricin, Zeocin, Hygromycin B were used in this study.

**Extraction of β-Carotene from *S. boulardii* Cultures.** Three replicates of each β-carotene producing *Sb* strain were inoculated into 1 mL CSM without uracil (2.5% glucose) and grown overnight in a shaking incubator at 250 rpm at 37 °C. Overnight cultures were then subinoculated (1:100) into 30 mL CSM without uracil (2.5% glucose) and grown for 3 days in a rotary incubator at 250 rpm at 37 °C. After 3 days, $2 \times 10^9$ cells were collected by centrifuging at 4 °C at 5000*g* for 5 min. The media was discarded and the cells were washed with 10 mL water and were centrifuged at 4 °C at 5000*g* for another 5 min. After the water was discarded, the cells were resuspended in 500 μL water and transferred into ZR Bashing Bead Tubes (Zymo Research, CA). The ZR Bashing tubes were centrifuged for 1 min at 8000*g* to discard the water. 500 μL acetone was then added into the bashing tubes. The tubes containing the cells, acetone, and lysis beads then transferred to a homogenizer (TissueLyser, Qiagen, Germany) for physical lysis (Lysis duration: 10 min, frequency: 30/s). The cells and the lysates then centrifuged at 16 000*g* for 5 min at 4 °C. The supernatants (acetone lysate) were transferred to 1.5 mL black microcentrifuge tubes. Fresh acetone was then added to the bashing tubes, and lysis steps were repeated 2 more times, at which point the cell pellets were completely white. β-carotene extracts were dried by speed vac (aqueous solvent, 30 °C for 2 h). Dried β-carotene pellets were reconstituted in 500 μL acetone and stored at −20 °C in the dark.

**Extraction of β-Carotene from Stool and Intestinal Samples.** Fecal and intestinal matter suspensions in PBS were centrifuged at 4500*g* for 20 min. PBS was removed from the fecal and intestinal matter pellets containing recombinant *Sb* cells. After the PBS was discarded, the pellets were resuspended in 1 mL 1× PBS and were transferred to ZR Bashing Bead Tubes (Zymo Research, CA). The ZR Bashing tubes were centrifuged for 1 min at 8000*g* to discard the water. 500 μL acetone was then added into the bashing tubes. The tubes containing the cells, acetone, and lysis beads then transferred to a homogenizer (TissueLyser, Qiagen, Germany) for physical lysis (Lysis duration: 10 min, frequency: 30/s). The cells and the lysates then centrifuged at 16 000*g* for 5 min at 4 °C. The supernatants (acetone lysate) were transferred to 1.5 mL black microcentrifuge tubes. Fresh acetone was then


https://doi.org/10.1021/acssynbio.0c00562
ACS Synth. Biol. 2021, 10, 1039−1052

added to the bashing tubes, and lysis steps were repeated 2 more times, at which point the extract solution was clear. Approximately 1.5 mL β-carotene extract solutions were obtained from each sample and the extract solutions were stored at −20 °C in the dark until the analysis.

**Detection of β-Carotene by HPLC.** *Cell Cultures.* 5 μL of each sample was processed in an Agilent 1260 Infinity high performance liquid-chromatography (HPLC) system (Agilent Technologies, CA, USA). 0.002 mM naphthalene solution was used as internal control and pure β-carotene (Thermo Fisher, Waltham, MA) at varying concentrations (mg/mL) 0.00625, 0.0125, 0.025, 0.05, 0.0625, 0.125, 0.25, 0.5, 0.625, 1.25, 2.5, 5) as external control. The channels used for internal control and β-carotene detection were 275 and 453 nm, respectively. The column used in the system was an Agilent HC-C28 Reversed Phase column (4.6 × 250 mm, 50 μL) (Agilent Technologies, CA, USA). The composition of the mobile phase was acetonitrile:methanol:isopropanol (v/v/v: 85/10/5) The flow rate for the mobile phase was 3 mL/min.

*Fecal and Intestinal Samples.* After all extractions, the samples were dried completely by nitrogen gas and then reconstituted with 400 μL high performance liquid-chromatography (HPLC)-grade acetone. A 250 μL sample of final extract was injected into the HPLC system (Ultimate 3000, Thermo Fisher, Waltham, MA). Pure β-carotene (Sigma-Aldrich, St. Louis, MO) at various concentrations (μM) 1, 5, 100, 500, 1000, 5000 was used as external control. The channel used for β-carotene detection was 475 nm. The column used in the system was Acclaim C30, 5 μm, 4.6 × 250 mm. The composition of the mobile phase was acetonitrile: methanol: methyl *tert*-butyl ether (v/v/v: 25:75:0 at time 0−20 min, 15:35:50 at time 20−25.5 min, 25:75:0 at time 25.5−30 min). The flow rate for the mobile phase was 1.0 mL/min.

## ■ ASSOCIATED CONTENT

### Supporting Information

The Supporting Information is available free of charge at https://pubs.acs.org/doi/10.1021/acssynbio.0c00562.

Supplementary figures, tables, and texts described throughout the manuscript (PDF)

Plasmid maps (ZIP)

Strains, plasmids, primers used in each figure (XLSX)

## ■ AUTHOR INFORMATION


### Corresponding Author

**Nathan Crook** − *Department of Chemical and Biomolecular Engineering, North Carolina State University, Raleigh, North Carolina 27695, United States;* orcid.org/0000-0001-6165-1972; Email: nccrook@ncsu.edu

### Authors

**Deniz Durmusoglu** − *Department of Chemical and Biomolecular Engineering, North Carolina State University, Raleigh, North Carolina 27695, United States*

**Ibrahim S. Al'Abri** − *Department of Chemical and Biomolecular Engineering, North Carolina State University, Raleigh, North Carolina 27695, United States*

**Scott P. Collins** − *Department of Chemical and Biomolecular Engineering, North Carolina State University, Raleigh, North Carolina 27695, United States*

**Junrui Cheng** − *Plants for Human Health Institute, North Carolina State University, Kannapolis, North Carolina 28081, United States*

**Abdulkerim Eroglu** − *Plants for Human Health Institute and Department of Molecular and Structural Biochemistry, College of Agriculture and Life Sciences, North Carolina State University, Kannapolis, North Carolina 28081, United States*

**Chase L. Beisel** − *Department of Chemical and Biomolecular Engineering, North Carolina State University, Raleigh, North Carolina 27695, United States; Helmholtz Institute for RNA-based Infection Research (HIRI), Helmholtz Centre for Infection Research (HZI), Würzburg 97080, Germany*

Complete contact information is available at: https://pubs.acs.org/10.1021/acssynbio.0c00562

### Author Contributions

⊥D.D. and I.S.A. contributed equally to this work


### Notes

The authors declare no competing financial interest.

## ■ ACKNOWLEDGMENTS

The authors gratefully acknowledge the assistance of Dr. Susan Tonkonogy and Karen Flores in performing germ-free mouse experiments in the Gnotobiotic Core at the College of Veterinary Medicine, North Carolina State University. The Core is supported by the National Institutes of Health funded Center for Gastrointestinal Biology and Disease, P30 DK034987. The authors thank Dr. Yong-Su Jin for kindly providing *S. boulardii* knockout strains. They thank the lab of Dr. Albert Keung for assistance with flow cytometry measurements. They thank the lab of Dr. Milad Abolhasani for assistance with HPLC experiments. They thank the lab of Dr. Robert Kelly for the use of their speed vac. They also thank Dr. John E. Dueber for kindly sharing the MoClo-YTK Toolkit and raw data. pLM494 was a gift from Bernd Müller-Röber (Addgene plasmid #100539). LbCas12a was a gift from the Roubos Lab (Addgene #101748). This work was supported by startup funds from North Carolina State University's Chemical and Biomolecular Engineering Department, the National Science Foundation (CBET-1934284), the Novo Nordisk Foundation (NNF19SA0035474), and the USDA National Institute of Food and Agriculture, [Hatch] project [accession no. #1021933]. D.D. and I.S.A. were supported by NCSU CBE startup funds. I.S.A. was also supported by the Ministry of Higher Education - Oman. A.E. and J.C. were supported by North Carolina State University startup funds. BioRender.com was used to make multiple figures in this manuscript.

## ■ REFERENCES

(1) O'Toole, P. W., Marchesi, J. R., and Hill, C. (2017) Next-Generation Probiotics: The Spectrum from Probiotics to Live Biotherapeutics. *Nat. Microbiol 2*, 17057.

(2) Mimee, M., Citorik, R. J., and Lu, T. K. (2016) Microbiome Therapeutics - Advances and Challenges. *Adv. Drug Delivery Rev. 105* (A), 44−54.

(3) Pedrolli, D. B., Ribeiro, N. V., Squizato, P. N., de Jesus, V. N., Cozetto, D. A., Tuma, R. B., Gracindo, A., Cesar, M. B., Freire, P. J.C., da Costa, A. F.M., Lins, M. R.C.R., Correa, G. G., and Cerri, M. O. (2019) Engineering Microbial Living Therapeutics: The Synthetic Biology Toolbox. *Trends Biotechnol. 37* (1), 100−115.

(4) Ozdemir, T., Fedorec, A. J. H., Danino, T., and Barnes, C. P. (2018) Synthetic Biology and Engineered Live Biotherapeutics: Toward Increasing System Complexity. *Cell Syst 7* (1), 5−16.

(5) Ferreiro, A., Crook, N., Gasparrini, A. J., and Dantas, G. (2018) Multiscale Evolutionary Dynamics of Host-Associated Microbiomes. *Cell 172* (6), 1216−1227.
(6) Bourdeau, R. W., Lee-Gosselin, A., Lakshmanan, A., Farhadi, A., Kumar, S. R., Nety, S. P., and Shapiro, M. G. (2018) Acoustic Reporter Genes for Noninvasive Imaging of Microorganisms in Mammalian Hosts. *Nature 553* (7686), 86−90.
(7) Riglar, D. T., Giessen, T. W., Baym, M., Kerns, S. J., Niederhuber, M. J., Bronson, R. T., Kotula, J. W., Gerber, G. K., Way, J. C., and Silver, P. A. (2017) Engineered Bacteria Can Function in the Mammalian Gut Long-Term as Live Diagnostics of Inflammation. *Nat. Biotechnol. 35* (7), 653−658.
(8) Kotula, J. W., Kerns, S. J., Shaket, L. A., Siraj, L., Collins, J. J., Way, J. C., and Silver, P. A. (2014) Programmable Bacteria Detect and Record an Environmental Signal in the Mammalian Gut. *Proc. Natl. Acad. Sci. U. S. A. 111* (13), 4838−4843.
(9) Shaw, W. M., Yamauchi, H., Mead, J., Gowers, G.-O. F., Bell, D. J., Öling, D., Larsson, N., Wigglesworth, M., Ladds, G., and Ellis, T. (2019) Engineering a Model Cell for Rational Tuning of GPCR Signaling. *Cell 177* (3), 782−796.
(10) Rugbjerg, P., and Sommer, M. O. A. (2019) Overcoming Genetic Heterogeneity in Industrial Fermentations. *Nat. Biotechnol. 37*, 869.
(11) Almeida, A., Mitchell, A. L., Boland, M., Forster, S. C., Gloor, G. B., Tarkowska, A., Lawley, T. D., and Finn, R. D. (2019) A New Genomic Blueprint of the Human Gut Microbiota. *Nature 568* (7753), 499−504.
(12) Sender, R., Fuchs, S., and Milo, R. (2016) Revised Estimates for the Number of Human and Bacteria Cells in the Body. *PLoS Biol. 14* (8), e1002533.
(13) Crook, N., Ferreiro, A., Gasparrini, A. J., Pesesky, M. W., Gibson, M. K., Wang, B., Sun, X., Condiotte, Z., Dobrowolski, S., Peterson, D., and Dantas, G. (2019) Adaptive Strategies of the Candidate Probiotic E. Coli Nissle in the Mammalian Gut. *Cell Host Microbe 25* (4), 499−512.
(14) Crook, N., Ferreiro, A., Condiotte, Z., and Dantas, G. (2020) Transcript Barcoding Illuminates the Expression Level of Synthetic Constructs in E. Coli Nissle Residing in the Mammalian Gut. *ACS Synth. Biol. 9* (5), 1010−1021.
(15) Isabella, V. M., Ha, B. N., Castillo, M. J., Lubkowicz, D. J., Rowe, S. E., Millet, Y. A., Anderson, C. L., Li, N., Fisher, A. B., West, K. A., Reeder, P. J., Momin, M. M., Bergeron, C. G., Guilmain, S. E., Miller, P. F., Kurtz, C. B., and Falb, D. (2018) Development of a Synthetic Live Bacterial Therapeutic for the Human Metabolic Disease Phenylketonuria. *Nat. Biotechnol. 36* (9), 857−864.
(16) Kurtz, C. B., Millet, Y. A., Puurunen, M. K., Perreault, M., Charbonneau, M. R., Isabella, V. M., Kotula, J. W., Antipov, E., Dagon, Y., Denney, W. S., Wagner, D. A., West, K. A., Degar, A. J., Brennan, A. M., and Miller, P. F. (2019) An Engineered E. Coli Nissle Improves Hyperammonemia and Survival in Mice and Shows Dose-Dependent Exposure in Healthy Humans. *Sci. Transl. Med. 11* (475), eaau7975.
(17) Ho, C. L., Tan, H. Q., Chua, K. J., Kang, A., Lim, K. H., Ling, K. L., Yew, W. S., Lee, Y. S., Thiery, J. P., and Chang, M. W. (2018) Engineered Commensal Microbes for Diet-Mediated Colorectal-Cancer Chemoprevention. *Nat. Biomed Eng. 2* (1), 27−37.
(18) Hwang, I. Y., Koh, E., Wong, A., March, J. C., Bentley, W. E., Lee, Y. S., and Chang, M. W. (2017) Engineered Probiotic Escherichia Coli Can. Eliminate and Prevent Pseudomonas Aeruginosa Gut Infection in Animal Models. *Nat. Commun. 8*, 15028.
(19) Sweere, J. M., Van Belleghem, J. D., Ishak, H., Bach, M. S., Popescu, M., Sunkari, V., Kaber, G., Manasherob, R., Suh, G. A., Cao, X., de Vries, C. R., Lam, D. N., Marshall, P. L., Birukova, M., Katznelson, E., Lazzareschi, D. V., Balaji, S., Keswani, S. G., Hawn, T. R., Secor, P. R., and Bollyky, P. L. (2019) Bacteriophage Trigger Antiviral Immunity and Prevent Clearance of Bacterial Infection. *Science 363* (6434), eaat9691.
(20) Brunk, E., Chang, R. L., Xia, J., Hefzi, H., Yurkovich, J. T., Kim, D., Buckmiller, E., Wang, H. H., Cho, B.-K., Yang, C., Palsson, B. O., Church, G. M., and Lewis, N. E. (2018) Characterizing Posttranslational Modifications in Prokaryotic Metabolism Using a Multiscale Workflow. *Proc. Natl. Acad. Sci. U. S. A. 115* (43), 11096−11101.
(21) Jiang, T. T., Shao, T.-Y., Ang, W. X. G., Kinder, J. M., Turner, L. H., Pham, G., Whitt, J., Alenghat, T., and Way, S. S. (2017) Commensal Fungi Recapitulate the Protective Benefits of Intestinal Bacteria. *Cell Host Microbe 22* (6), 809−816.
(22) Huseyin, C. E., O'Toole, P. W., Cotter, P. D., and Scanlan, P. D. (2017) Forgotten Fungi-the Gut Mycobiome in Human Health and Disease. *FEMS Microbiol. Rev. 41* (4), 479−511.
(23) Wheeler, M. L., Limon, J. J., Bar, A. S., Leal, C. A., Gargus, M., Tang, J., Brown, J., Funari, V. A., Wang, H. L., Crother, T. R., Arditi, M., Underhill, D. M., and Iliev, I. D. (2016) Immunological Consequences of Intestinal Fungal Dysbiosis. *Cell Host Microbe 19* (6), 865−873.
(24) Hamad, I., Ranque, S., Azhar, E. I., Yasir, M., Jiman-Fatani, A. A., Tissot-Dupont, H., Raoult, D., and Bittar, F. (2017) Culturomics and Amplicon-Based Metagenomic Approaches for the Study of Fungal Population in Human Gut Microbiota. *Sci. Rep. 7* (1), 16788.
(25) Richard, M. L., and Sokol, H. (2019) The Gut Mycobiota: Insights into Analysis, Environmental Interactions and Role in Gastrointestinal Diseases. *Nat. Rev. Gastroenterol. Hepatol. 16* (6), 331−345.
(26) Shao, T.-Y., Ang, W. X. G., Jiang, T. T., Huang, F. S., Andersen, H., Kinder, J. M., Pham, G., Burg, A. R., Ruff, B., Gonzalez, T., Khurana Hershey, G. K., Haslam, D. B., and Way, S. S. (2019) Commensal Candida Albicans Positively Calibrates Systemic Th17 Immunological Responses. *Cell Host Microbe 25* (3), 404−417.
(27) Tso, G. H. W., Reales-Calderon, J. A., Tan, A. S. M., Sem, X., Le, G. T. T., Tan, T. G., Lai, G. C., Srinivasan, K. G., Yurieva, M., Liao, W., Poidinger, M., Zolezzi, F., Rancati, G., and Pavelka, N. (2018) Experimental Evolution of a Fungal Pathogen into a Gut Symbiont. *Science 362* (6414), 589−595.
(28) Hotel, A. C. P., and Cordoba, A. (2001) Health and Nutritional Properties of Probiotics in Food Including Powder Milk with Live Lactic Acid Bacteria. *Prevention 5* (1), 1−10.
(29) van der Aa Kühle, A., and Jespersen, L. (2003) The Taxonomic Position of Saccharomyces Boulardii as Evaluated by Sequence Analysis of the D1/D2 Domain of 26S RDNA, the ITS1−5.8S RDNA-ITS2 Region and the Mitochondrial Cytochrome-c Oxidase II Gene. *Syst. Appl. Microbiol. 26* (4), 564−571.
(30) Tiago, F. C. P., Martins, F. S., Souza, E. L. S., Pimenta, P. F. P., Araujo, H. R. C., Castro, I. M., Brandão, R. L., and Nicoli, J. R. (2012) Adhesion to the Yeast Cell Surface as a Mechanism for Trapping Pathogenic Bacteria by Saccharomyces Probiotics. *J. Med. Microbiol. 61* (9), 1194−1207.
(31) Hudson, L. E., McDermott, C. D., Stewart, T. P., Hudson, W. H., Rios, D., Fasken, M. B., Corbett, A. H., and Lamb, T. J. (2016) Characterization of the Probiotic Yeast Saccharomyces Boulardii in the Healthy Mucosal Immune System. *PLoS One 11* (4), e0153351.
(32) Khatri, I., Tomar, R., Ganesan, K., Prasad, G. S., and Subramanian, S. (2017) Complete Genome Sequence and Comparative Genomics of the Probiotic Yeast Saccharomyces Boulardii. *Sci. Rep. 7* (1), 371.
(33) Liu, J.-J., Kong, I. I., Zhang, G.-C., Jayakody, L. N., Kim, H., Xia, P.-F., Kwak, S., Sung, B. H., Sohn, J.-H., Walukiewicz, H. E., Rao, C. V., and Jin, Y.-S. (2016) Metabolic Engineering of Probiotic Saccharomyces Boulardii. *Appl. Environ. Microbiol. 82* (8), 2280−2287.
(34) Fietto, J. L. R., Araújo, R. S., Valadão, F. N., Fietto, L. G., Brandão, R. L., Neves, M. J., Gomes, F. C. O., Nicoli, J. R., and Castro, I. M. (2004) Molecular and Physiological Comparisons between Saccharomyces Cerevisiae and Saccharomyces Boulardii. *Can. J. Microbiol. 50* (8), 615−621.
(35) Rodrigues, A. C. P., Cara, D. C., Fretez, S. H. G. G., Cunha, F. Q., Vieira, E. C., Nicoli, J. R., and Vieira, L. Q. (2000) Saccharomyces Boulardii Stimulates SIgA Production and the Phagocytic System of Gnotobiotic Mice: Immunomodulation by Probiotic. *J. Appl. Microbiol. 89* (3), 404−414.


https://doi.org/10.1021/acssynbio.0c00562
*ACS Synth. Biol.* 2021, 10, 1039−1052

(36) Palma, M. L., Garcia-Bates, T. M., Martins, F. S., and Douradinha, B. (2019) Genetically Engineered Probiotic Saccharomyces Cerevisiae Strains Mature Human Dendritic Cells and Stimulate Gag-Specific Memory CD8+ T Cells Ex Vivo. *Appl. Microbiol. Biotechnol. 103* (13), 5183−5192.
(37) Chen, K., Zhu, Y., Zhang, Y., Hamza, T., Yu, H., Saint Fleur, A., Galen, J., Yang, Z., and Feng, H. (2020) A Probiotic Yeast-Based Immunotherapy against Clostridioides Difficile Infection. *Sci. Transl. Med. 12* (567), eaax4905.
(38) Michael, S., Keubler, L. M., Smoczek, A., Meier, M., Gunzer, F., Pöhlmann, C., Krause-Buchholz, U., Hedrich, H.-J., and Bleich, A. (2013) Quantitative Phenotyping of Inflammatory Bowel Disease in the IL-10-Deficient Mouse by Use of Noninvasive Magnetic Resonance Imaging. *Inflamm. Bowel Dis. 19* (1), 185−193.
(39) Liu, C.-H., Chang, J.-H., Chang, Y.-C., and Mou, K. Y. (2020) Treatment of Murine Colitis by Saccharomyces Boulardii Secreting Atrial Natriuretic Peptide. *J. Mol. Med. 98*, 1675.
(40) Żymańczyk-Duda, E., Brzezińska-Rodak, M., Klimek-Ochab, M., Duda, M., and Zerka, A. (2017) Yeast as a Versatile Tool in Biotechnology. In *Yeast—Industrial Applications* (Morata, A., and Loira, I., Eds.) InTech, London, England.
(41) Lee, M. E., DeLoache, W. C., Cervantes, B., and Dueber, J. E. (2015) A Highly Characterized Yeast Toolkit for Modular, Multipart Assembly. *ACS Synth. Biol. 4* (9), 975−986.
(42) Karim, A. S., Curran, K. A., and Alper, H. S. (2013) Characterization of Plasmid Burden and Copy Number in Saccharomyces Cerevisiae for Optimization of Metabolic Engineering Applications. *FEMS Yeast Res. 13* (1), 107−116.
(43) Xiao, Y., Bowen, C. H., Liu, D., and Zhang, F. (2016) Exploiting Nongenetic Cell-to-Cell Variation for Enhanced Biosynthesis. *Nat. Chem. Biol. 12* (5), 339−344.
(44) Mundt, M., Anders, A., Murray, S. M., and Sourjik, V. (2018) A System for Gene Expression Noise Control in Yeast. *ACS Synth. Biol. 7* (11), 2618−2626.
(45) Crook, N. C., Freeman, E. S., and Alper, H. S. (2011) Re-Engineering Multicloning Sites for Function and Convenience. *Nucleic Acids Res. 39* (14), e92.
(46) Newman, J. R. S., Ghaemmaghami, S., Ihmels, J., Breslow, D. K., Noble, M., DeRisi, J. L., and Weissman, J. S. (2006) Single-Cell Proteomic Analysis of S. Cerevisiae Reveals the Architecture of Biological Noise. *Nature 441* (7095), 840−846.
(47) Duveau, F., Hodgins-Davis, A., Metzger, B. P., Yang, B., Tryban, S., Walker, E. A., Lybrook, T., and Wittkopp, P. J. (2018) Fitness Effects of Altering Gene Expression Noise in Saccharomyces Cerevisiae. *eLife*, DOI: 10.7554/eLife.37272.
(48) Aranda-Díaz, A., Mace, K., Zuleta, I., Harrigan, P., and El-Samad, H. (2017) Robust Synthetic Circuits for Two-Dimensional Control of Gene Expression in Yeast. *ACS Synth. Biol. 6* (3), 545−554.
(49) Datta, S., Annapure, U. S., and Timson, D. J. (2017) Different Specificities of Two Aldehyde Dehydrogenases from Saccharomyces Cerevisiae Var. Boulardii. *Biosci. Rep.*, DOI: 10.1042/BSR20160529.
(50) Elledge, S. J., and Davis, R. W. (1987) Identification and Isolation of the Gene Encoding the Small Subunit of Ribonucleotide Reductase from Saccharomyces Cerevisiae: DNA Damage-Inducible Gene Required for Mitotic Viability. *Mol. Cell. Biol. 7* (8), 2783−2793.
(51) Curran, K. A., Karim, A. S., Gupta, A., and Alper, H. S. (2013) Use of Expression-Enhancing Terminators in Saccharomyces Cerevisiae to Increase MRNA Half-Life and Improve Gene Expression Control for Metabolic Engineering Applications. *Metab. Eng. 19*, 88−97.
(52) Wei, L., Wang, Z., Zhang, G., and Ye, B. (2017) Characterization of Terminators in Saccharomyces Cerevisiae and an Exploration of Factors Affecting Their Strength. *ChemBioChem 18* (24), 2422−2427.
(53) Yamanishi, M., Ito, Y., Kintaka, R., Imamura, C., Katahira, S., Ikeuchi, A., Moriya, H., and Matsuyama, T. (2013) A Genome-Wide Activity Assessment of Terminator Regions in Saccharomyces Cerevisiae Provides a "terminatome" Toolbox. *ACS Synth. Biol. 2* (6), 337−347.
(54) Reider Apel, A., d'Espaux, L., Wehrs, M., Sachs, D., Li, R. A., Tong, G. J., Garber, M., Nnadi, O., Zhuang, W., Hillson, N. J., Keasling, J. D., and Mukhopadhyay, A. (2017) A Cas9-Based Toolkit to Program Gene Expression in Saccharomyces Cerevisiae. *Nucleic Acids Res. 45* (1), 496−508.
(55) Struhl, K., and Segal, E. (2013) Determinants of Nucleosome Positioning. *Nat. Struct. Mol. Biol. 20* (3), 267−273.
(56) Raschmanová, H., Weninger, A., Glieder, A., Kovar, K., and Vogl, T. (2018) Implementing CRISPR-Cas Technologies in Conventional and Non-Conventional Yeasts: Current State and Future Prospects. *Biotechnol. Adv. 36* (3), 641−665.
(57) Flagfeldt, D. B., Siewers, V., Huang, L., and Nielsen, J. (2009) Characterization of Chromosomal Integration Sites for Heterologous Gene Expression in Saccharomyces Cerevisiae. *Yeast 26* (10), 545−551.
(58) Siddiqui, M. S., Choksi, A., and Smolke, C. D. (2014) A System for Multilocus Chromosomal Integration and Transformation-Free Selection Marker Rescue. *FEMS Yeast Res. 14* (8), 1171−1185.
(59) Verwaal, R., Buiting-Wiessenhaan, N., Dalhuijsen, S., and Roubos, J. A. (2018) CRISPR/Cpf1 Enables Fast and Simple Genome Editing of Saccharomyces Cerevisiae. *Yeast 35* (2), 201−211.
(60) Yuan, J., and Ching, C. B. (2015) Combinatorial Assembly of Large Biochemical Pathways into Yeast Chromosomes for Improved Production of Value-Added Compounds. *ACS Synth. Biol. 4* (1), 23−31.
(61) Lee, M. E., Aswani, A., Han, A. S., Tomlin, C. J., and Dueber, J. E. (2013) Expression-Level Optimization of a Multi-Enzyme Pathway in the Absence of a High-Throughput Assay. *Nucleic Acids Res. 41* (22), 10668−10678.
(62) Wingler, L. M., and Cornish, V. W. (2011) Reiterative Recombination for the in Vivo Assembly of Libraries of Multigene Pathways. *Proc. Natl. Acad. Sci. U. S. A. 108* (37), 15135−15140.
(63) Choi, S. Y., Yoon, K.-H., Lee, J. I., and Mitchell, R. J. (2015) Violacein: Properties and Production of a Versatile Bacterial Pigment. *BioMed Res. Int. 2015*, 1−8.
(64) Verwaal, R., Wang, J., Meijnen, J.-P., Visser, H., Sandmann, G., van den Berg, J. A., and van Ooyen, A. J. J. (2007) High-Level Production of Beta-Carotene in Saccharomyces Cerevisiae by Successive Transformation with Carotenogenic Genes from Xanthophyllomyces Dendrorhous. *Appl. Environ. Microbiol. 73* (13), 4342−4350.
(65) Cunningham, F. X., and Gantt, E. (2001) One Ring or Two? Determination of Ring Number in Carotenoids by Lycopene ε-Cyclases. *Proc. Natl. Acad. Sci. U. S. A. 98* (5), 2905−2910.
(66) Blehaut, H., Massot, J., Elmer, G. W., and Levy, R. H. (1989) Disposition Kinetics of Saccharomyces Boulardii in Man and Rat. *Biopharm. Drug Dispos. 10* (4), 353−364.
(67) Barc, M.-C., Charrin-Sarnel, C., Rochet, V., Bourlioux, F., Sandré, C., Boureau, H., Doré, J., and Collignon, A. (2008) Molecular Analysis of the Digestive Microbiota in a Gnotobiotic Mouse Model during Antibiotic Treatment: Influence of Saccharomyces Boulardii. *Anaerobe 14* (4), 229−233.
(68) Kennedy, E. A., King, K. Y., and Baldridge, M. T. (2018) Mouse Microbiota Models: Comparing Germ-Free Mice and Antibiotics Treatment as Tools for Modifying Gut Bacteria. *Front. Physiol. 9*, 1534.
(69) Shah, P., Fritz, J. V., Glaab, E., Desai, M. S., Greenhalgh, K., Frachet, A., Niegowska, M., Estes, M., Jäger, C., Seguin-Devaux, C., Zenhausern, F., and Wilmes, P. (2016) A Microfluidics-Based in Vitro Model of the Gastrointestinal Human-Microbe Interface. *Nat. Commun. 7* (1), 11535.
(70) Costello, C. M., Sorna, R. M., Goh, Y.-L., Cengic, I., Jain, N. K., and March, J. C. (2014) 3-D Intestinal Scaffolds for Evaluating the Therapeutic Potential of Probiotics. *Mol. Pharmaceutics 11* (7), 2030−2039.
(71) Esch, M. B., Sung, J. H., Yang, J., Yu, C., Yu, J., March, J. C., and Shuler, M. L. (2012) On Chip Porous Polymer Membranes for

Integration of Gastrointestinal Tract Epithelium with Microfluidic "body-on-a-Chip" Devices. *Biomed. Microdevices 14* (5), 895−906.
(72) Kim, W., and Kim, G. H. (2018) An Innovative Cell-Printed Microscale Collagen Model for Mimicking Intestinal Villus Epithelium. *Chem. Eng. J. 334*, 2308−2318.
(73) Williams, C. F., Walton, G. E., Jiang, L., Plummer, S., Garaiova, I., and Gibson, G. R. (2015) Comparative Analysis of Intestinal Tract Models. *Annu. Rev. Food Sci. Technol. 6* (1), 329−350.
(74) Poeker, S. A., Lacroix, C., de Wouters, T., Spalinger, M. R., Scharl, M., and Geirnaert, A. (2019) Stepwise Development of an in Vitro Continuous Fermentation Model for the Murine Caecal Microbiota. *Front. Microbiol. 10*, 1166.
(75) Rose, C., Parker, A., Jefferson, B., and Cartmell, E. (2015) The Characterization of Feces and Urine: A Review of the Literature to Inform Advanced Treatment Technology. *Crit. Rev. Environ. Sci. Technol. 45* (17), 1827−1879.
(76) Trumbo, P., Yates, A. A., Schlicker, S., and Poos, M. (2001) Dietary Reference Intakes: Vitamin A, Vitamin K, Arsenic, Boron, Chromium, Copper, Iodine, Iron, Manganese, Molybdenum, Nickel, Silicon, Vanadium, and Zinc. *J. Am. Diet. Assoc. 101* (3), 294−301.
(77) Auci, D. L., Egilmez, N. K., and Dryden, G. W. (2018) Anti-Fibrotic Potential of All Trans Retinoic Acid in Inflammatory Bowel Disease. *J. Gastroenterol. Pancreatol. Liver Disord. 6* (3), 1.
(78) Priyamvada, S., Anbazhagan, A. N., Kumar, A., Chatterjee, I., Borthakur, A., Saksena, S., Gill, R. K., Alrefai, W. A., and Dudeja, P. K. (2020) All-Trans Retinoic Acid Counteracts Diarrhea and Inhibition of Downregulated in Adenoma Expression in Gut Inflammation. *Inflamm. Bowel Dis. 26* (4), 534−545.
(79) Lee, J. J. L., Chen, L., Cao, B., and Chen, W. N. (2016) Engineering Rhodosporidium Toruloides with a Membrane Transporter Facilitates Production and Separation of Carotenoids and Lipids in a Bi-Phasic Culture. *Appl. Microbiol. Biotechnol. 100* (2), 869−877.
(80) Verwaal, R., Jiang, Y., Wang, J., Daran, J.-M., Sandmann, G., van den Berg, J. A., and van Ooyen, A. J. J. (2010) Heterologous Carotenoid Production in Saccharomyces Cerevisiae Induces the Pleiotropic Drug Resistance Stress Response. *Yeast 27* (12), 983−998.
(81) Potapov, V., Ong, J. L., Kucera, R. B., Langhorst, B. W., Bilotti, K., Pryor, J. M., Cantor, E. J., Canton, B., Knight, T. F., Evans, T. C., Jr, and Lohman, G. J. S. (2018) Comprehensive Profiling of Four Base Overhang Ligation Fidelity by T4 DNA Ligase and Application to DNA Assembly. *ACS Synth. Biol. 7* (11), 2665−2674.
(82) Gietz, R D., and Schiestl, R. H (2007) High-Efficiency Yeast Transformation Using the LiAc/SS Carrier DNA/PEG Method. *Nat. Protoc. 2*, 31−34.
(83) Gietz, R D., and Schiestl, R. H (2007) Quick and Easy Yeast Transformation Using the LiAc/SS Carrier DNA/PEG Method. *Nat. Protoc. 2*, 35−37.


https://doi.org/10.1021/acssynbio.0c00562
*ACS Synth. Biol.* 2021, 10, 1039−1052